MOLECULAR IMAGING AND BIOLOGY

Mol Imaging Biol (2019) 21:620–625
DOI: 10.1007/s11307-018-1291-y

Published Online: 1 November 2018

BRIEF ARTICLE

Characterization of Brown Adipose Tissue in a Diabetic Mouse Model with Spiral Volumetric Optoacoustic Tomography

Avihai Ron, Xosé Luís Deán-Ben, Josephine Reber, Vasilis Ntziachristos, Daniel Razansky

Institute for Biological and Medical Imaging, Technical University of Munich and Helmholtz Center Munich, Munich, Germany

Abstract

Purpose: Diabetes is associated with a deterioration of the microvasculature in brown adipose tissue (BAT) and with a decrease in its metabolic activity. Multispectral optoacoustic tomography has been recently proposed as a new tool capable of differentiating healthy and diabetic BAT by observing hemoglobin gradients and microvasculature density in cross-sectional (2D) views. We report on the use of spiral volumetric optoacoustic tomography (SVOT) for an improved characterization of BAT.

Procedures: A streptozotocin-induced diabetes model and control mice were scanned with SVOT. Volumetric oxygen saturation (sO_2) as well as total blood volume (TBV) in the subcutaneous interscapular BAT (iBAT) was quantified. Segmentation further enabled separating feeding and draining vessels from the BAT anatomical structure.

Results: Scanning revealed a 46 % decrease in TBV and a 25 % decrease in sO_2 in the diabetic iBAT with respect to the healthy control.

Conclusions: These results suggest that SVOT may serve as an effective tool for studying the effects of diabetes on BAT. The volumetric optoacoustic imaging probe used for the SVOT scans can be operated in a handheld mode, thus potentially providing a clinical translation route for BAT-related studies with this imaging technology.

Key words: Optoacoustic, Brown fat, Metabolism, Hemoglobin, Oxygen saturation, Adipose tissue, Angiopathy

Introduction

Brown adipose tissue (BAT) appears to provide a self-defense mechanism against diabetes and has been shown to offer therapeutic potential against this widespread disease [1]. BAT has long been recognized to play a role in temperature control in newborns. Yet, recent evidence suggests that it is also present and active in adults [2], primarily located behind the muscles of the lower neck and collarbone [3]. In diabetic patients, a decrease in the metabolic activity of BAT has been observed [4], which appears to correlate with angiopathy [5]. Mouse models have shown promise in facilitating studies into the BAT metabolism [6], further supported by wide availability of the diabetes models [7, 8]. In mice, BAT is spread across several locations, primarily in the cervical-thoracic region, known as the subcutaneous interscapular BAT (iBAT).

Accurate non-invasive characterization of BAT and its metabolic activity may greatly facilitate development of novel strategies to treat diabetes. The presence of BAT and

Electronic supplementary material The online version of this article (https://doi.org/10.1007/s11307-018-1291-y) contains supplementary material, which is available to authorized users.

Correspondence to: Daniel Razansky; *e-mail:* dr@tum.de

its metabolism can be characterized by glucose uptake rate as measured by 2-deoxy-2-[^{18}F]fluoro -D-glucose [9–11], translocator proteins [12], or cannabinoid receptor-1 [13] tracers in positron emission tomography. The use of ionizing radiation however impedes longitudinal clinical studies while further involving introduction of exogenous agents. On the other hand, tissue blood flow can be estimated by contrast-enhanced ultrasound [14] and near-infrared fluorescent imaging [15], thus providing an indirect measure of metabolic activity. Another potential indicator of such activity is elevated tissue temperature, which can only be measured superficially with infrared imaging [16]. The limitations of existing imaging approaches urge therefore for the development of new approaches for the characterization of BAT and its metabolic activity.

Multispectral optoacoustic tomography (MSOT) has previously shown promise for non-invasive label-free measurements of iBAT metabolism and differentiation between its diabetic and healthy states by imaging of hemoglobin gradients and blood volume [17]. MSOT-based detection of development of beige adipocytes during adrenergic stimulation was further demonstrated using expression of near-infrared fluorescence protein iRFP720 [18]. Spiral volumetric optoacoustic tomography (SVOT) has recently offered unprecedented capabilities for three-dimensional (3D) characterization of microvascular structures and oxygen saturation (sO_2) quantification in whole mice [19]. Here, we investigate the SVOT capabilities for the 3D visualization and characterization of entire iBAT depots in healthy and diabetic mice.

Materials and Methods

The SVOT Imaging System

A schematic representation of the SVOT scanning procedure is provided in Fig. 1a with a more detailed description available elsewhere [19]. Briefly, a spherical ultrasound array of piezocomposite elements is mounted on motorized rotating and translating stages and scanned around the mouse following a helical (spiral) trajectory. The array consists of 256 elements with a central frequency of 4 MHz and – 6 dB bandwidth of ~ 100 % distributed on a spherical surface with 40 mm radius and 90° angular coverage. Optical excitation is provided by short-pulsed laser light (10 ns duration pulses with 25 mJ per-pulse energy and up to 100 Hz pulse repetition frequency) tunable in the near-infrared range (700–900 nm). Light is guided *via* a fiber bundle through a central aperture of the array. SVOT enables imaging the entire mouse with a nearly isotropic 3D spatial resolution in the 300 µm range [20].

In vivo Experiments

Male BALB/c mice (6–8 weeks old, Envigo Laboratories, Germany) were kept at 24 ± 1 °C on a 12:12-h light-dark cycle and fed with standard rodent diet (Altromin 1314, Altromin Spezialfutter GmbH & Co, Germany) with free access to water. Diabetes was induced with a single intraperitoneal injection of streptozotocin (Sigma, Germany) at 150 mg/kg body weight after 4–6 h fasting. Blood glucose levels (350–500 mg/dl) were measured on the same day when the SVOT scanning was performed, 7–14 days after induction of diabetes. Prior to *in vivo* imaging, the mice were anesthetized with isoflurane, placed in a custom-made animal holder, and immersed in a water tank (water temperature 33 °C) to facilitate efficient propagation and detection of the optoacoustically generated pressure waves. The head of the animals was kept above water, and a mask was placed over the mouth and nose for the administration of anesthesia and oxygen. All *in vivo* mouse experiments were performed in full compliance with the institutional guidelines of the Helmholtz Center Munich and with approval from the Government District of Upper Bavaria.

Data Analysis

SVOT imaging of mice was performed in a localized region surrounding the iBAT. The tomographic optoacoustic data was acquired at four wavelengths, namely, 730, 760, 800, and 850 nm. Tomographic reconstructions of single volumes ($15 \times 15 \times 15$ mm^3) for each scanning position of the spherical array transducer were done using a 3D back-projection-based algorithm [21, 22] implemented in MATLAB (MathWorks, USA). Volumetric image frames associated with breathing motion were identified and removed for an enhanced imaging performance, as previously reported [20]. All remaining frames were subsequently averaged and the resulting images were corrected for exponential light attenuation with depth according to $e^{-\sqrt{3\mu_a(\lambda)(\mu_a(\lambda)+\mu'_s(\lambda))}z}$, where average values for the wavelength-dependent reduced scattering $\mu_s'(\lambda)$ and absorption $\mu_a(\lambda)$ coefficients in adipose tissue were taken from literature [23]. All individual reconstructions were then combined based on the known positions of the ultrasound array during the SVOT scan [20]. Microvasculature density was estimated from the total blood volume (TBV) in the iBAT region, which was calculated from the voxel intensity values of the reconstructed images at 800 nm excitation (isosbestic point of hemoglobin). A standard linear spectral unmixing algorithm [24] was applied to the multispectral data on a voxel-by-voxel basis to retrieve the bio-distribution of HbO_2 and Hb. The blood oxygen saturation (sO_2) was then calculated as the ratio between the HbO_2 and the sum of the HbO_2 and Hb signals. A Mann-Whitney test was used for statistical comparisons between the groups. All processing procedures were performed in MATLAB and the final 3D images were exported into Amira (Thermo Fisher Scientific, USA) for better visualization.

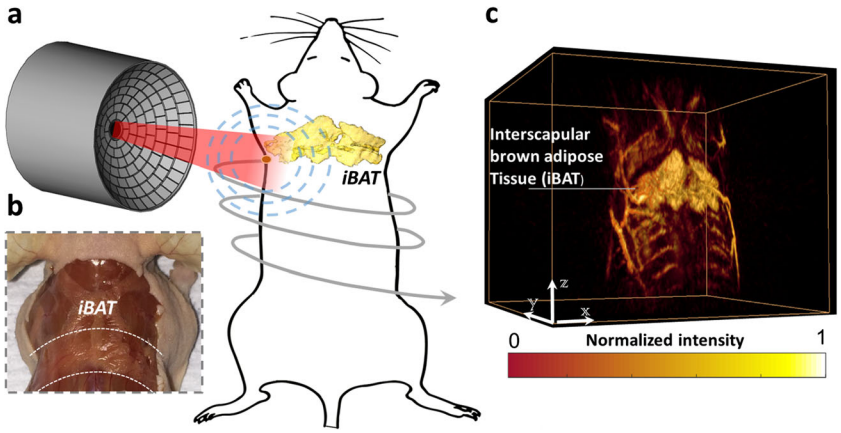

Fig. 1. **a** Schematics of the SVOT system. Light is emitted from the center of the spherical transducer array, which detects the optoacoustic signal. The transducer array rotates in a spiral motion around the animal. **b** A photo of the skin of the lower neck region removed, exposing the iBAT. **c** A 3D representation of a SVOT scan of the lower neck region, clearly showing the iBAT in a mouse.

Data Availability

The datasets used and/or analyzed during the current study are available from the corresponding author on reasonable request.

Results

The anatomical position of iBAT can be clearly discerned within the interscapular region (Fig. 1b) in the whole-body SVOT images taken at 800 nm (Fig. 1c). This large-area scan was performed with 10 angular positions (10° step) and 8 translational positions (2 mm step) of the array, resulting in a highly detailed (200 µm spatial resolution) 3D image of the entire thoracic region of the mouse. The high contrast generated by the system from the iBAT is primarily associated with the rich and dense microvasculature of this tissue [25].

The iBAT regions of the healthy ($n = 3$) and the streptozotocin-induced, diabetic mice ($n = 3$) were then scanned multispectrally. The iBAT can be easily spotted anatomically in the images taken at the isosbestic hemoglobin wavelength of 800 nm, effectively representing the total blood volume (TBV) distribution (Fig. 2a). The main draining vein from the iBAT, the so-called Sulzer vein (SV), is also visible. The expected deterioration of the microvasculature density in the diabetic iBAT is consistent with the observed 46 % lower TBV value as compared to the healthy control (Fig. 2b).

Spectral unmixing of the multiwavelength image data further revealed the sO_2 distribution in the iBAT (Fig. 3.a). To quantify the TBV and sO_2 values in the iBAT independently from the large vessels, a global threshold for the sO_2 map was set automatically by using the Otsu's method [26]. This threshold value of 60 % sO_2 was applied to the sO_2 map in order to set iBAT apart from the surrounding large vessels (Fig. 3.b). When comparing with average oxygenation levels of the healthy iBAT ($sO_2 =$ 36 %), the decreased metabolic activity in the diabetic iBAT results in reduced sO_2 levels of $sO_2 = 27$ % (Fig. 3.c). The separation between the mean sO_2 values for the healthy and diabetic groups is also evident based on individual animal data (Suppl. Fig. S1). The large vessels, on the other hand, show slightly decreased average oxygenation levels in diabetic mice ($sO_2 = 75$ %) as compared to the healthy controls ($sO_2 = 78$ %).

Discussion

We performed a straightforward quantification of sO_2 in the entire iBAT depots. The results support the MSOT measurements of metabolic activity [17], both in terms of the sO_2 trends and decrease of TBV in diabetic mice. Yet, the SVOT images enable better visualization of the depots and arguably more quantitative measurements due to the full 3D tomographic angular coverage and nearly isotropic resolution in all three dimensions [19]. Vascular structures can be clearly identified in the SVOT scans, which may facilitate the registration of images taken at different time points in longitudinal studies of the effects of diabetes on BAT.

The decrease in sO_2 of iBAT observed in diabetic mice is consistent with the expected decrease in metabolic activity in this tissue. The SVOT method is uniquely endowed with the capacity for longitudinal tracking of deep tissue oxygen metabolism without the need for extrinsic labeling. Its high sensitivity to hemoglobin allows for high-contrast visualization of the iBAT depots containing dense microvasculature networks. The measured reduced TBV values in the diabetic iBAT imply a decrease in the vasculature density with respect to the healthy tissue. Such deficiency is generally expected due to angiopathy-related vasculature deterioration. The sO_2 quantification can be significantly hampered if the iBAT cannot be clearly separated from the surrounding vessels, which was readily achieved here based on large differences in their underlying sO_2 levels.

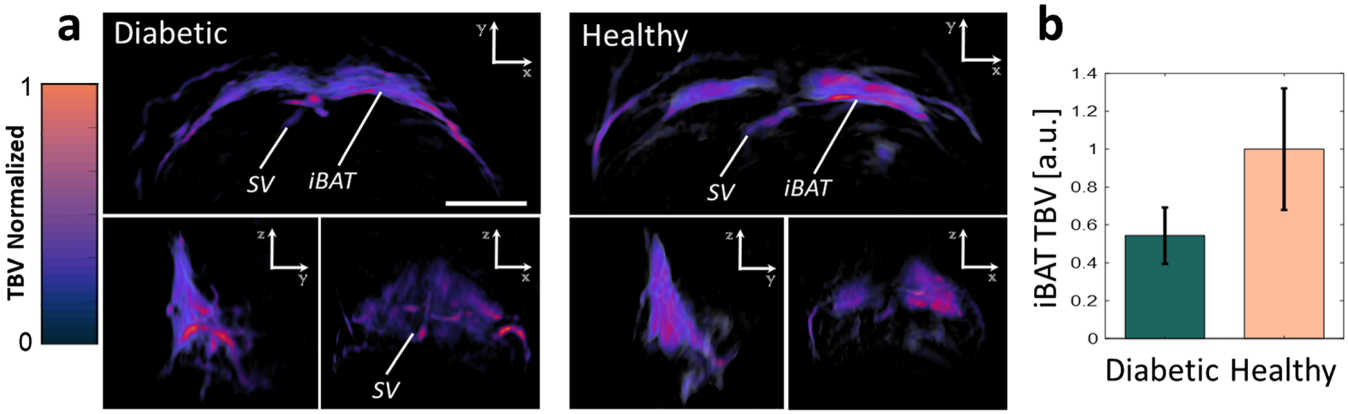

Fig. 2. **a** Three maximal intensity projections of the TBV distribution in the iBAT region of a diabetic mouse and a healthy mouse. The Sulzer vein (SV) position is also marked. **b** Comparison of TBV distribution in the diabetic and healthy iBAT ($p < 0.01$).

It has been previously shown that SVOT allows for visualizing biological processes at temporal scales ranging from a few milliseconds to several days [19]. Hence, apart from longitudinal studies on diabetes, it might further be possible to image dynamics in the iBAT depots, *e.g.*, associated with the induced activation of BAT [17]. The true volumetric nature of SVOT offers several advantages with respect to other commonly employed cross-sectional optoacoustic imaging approaches [27, 28]. Indeed, the large solid angular coverage provided by the spherical array transducer enables accurate three-dimensional reconstructions not afflicted by the so-called limited-view effects [29]. This facilitates enhanced visibility of the three-dimensional tissue morphology and more quantitative readings of the

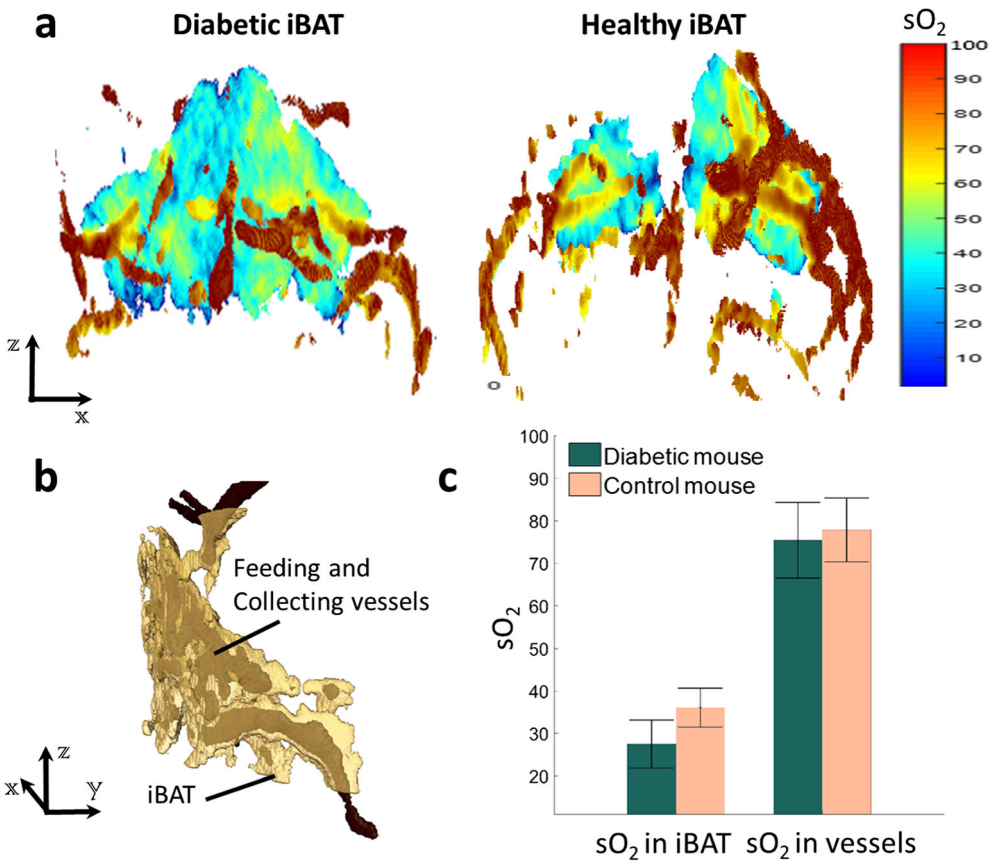

Fig. 3. **a** Coronal projection of the sO_2 distribution map of the iBAT region of a diabetic mouse and a healthy mouse. **b** An illustration of the segmented iBAT in semi-transparent yellow, exposing feeding and collecting vessels in red, interwoven between and around the iBAT. **c** Comparison of sO_2 distribution between healthy and diabetic iBAT ($p < 0.01$) and between their major vessels.

tissue biochromes. Spatial resolution of the SVOT observations can also be enhanced by employing a spherical array with a larger detection bandwidth, as has recently been showcased with the optoacoustic microtomography (OMT) method [30]. At the near-infrared wavelengths, structures at a depth of at least 1 cm in living tissues can be imaged by SVOT, although this limitation is less significant in our measurements owing to the superficial location and high vascularization of the iBAT.

Conclusions

This work illustrates capabilities of the SVOT technique in diabetic research. Our results corroborate and complement recently reported measurements of metabolic activity where oxy and deoxy-hemoglobin gradients measured by a cross-sectional MSOT technique were used to differentiate between healthy and diabetic iBAT in mice [17]. Finally, the volumetric optoacoustic imaging probe used for the SVOT scans can be seamlessly operated in a handheld mode [31]. Since cervical BAT is located relatively superficially in humans, it is expected to be readily accessible with a handheld optoacoustic system based on a spherical matrix array. This may potentially serve as a viable clinical translation route for BAT-related studies with this 3D imaging technology. All in all, the volumetric and dynamic imaging capabilities of SVOT have the potential to reveal new insights into the BAT metabolism and improve its characterization in diabetes research.

Acknowledgements. The authors wish to thank Mr. Uwe Klemm and Mr. Michael Reiss for their support with animal handling.

Funding Information. The work leading to these results was partially supported by the Human Frontier Science Program (HFSP) Grant RGY0070/201 and the European Research Council Grant ERC-2015-CoG-682379. Support from the Deutsche Forschungsgemeinschaft (DFG), Germany [Gottfried Wilhelm Leibniz Prize 2013; NT 3/10-1], and from the European Research Council (ERC) under grant agreement No 694968 (PREMSOT) is further acknowledged.

Compliance with Ethical Standards

Ethics Approval and Consent to Participate

Not applicable.

Consent for Publication

Not applicable.

Conflict of Interest

The authors declare that they have no conflict of interest.

References

1. Owens B (2014) The changing colour of fat. Nature 508(7496):S52–S53
2. Nedergaard J, Bengtsson T, Cannon B (2007) Unexpected evidence for active brown adipose tissue in adult humans. Am J Physiol-Endoc Metab 293:E444–E452
3. Enerbäck S (2010) Human brown adipose tissue. Cell Metab 11:248–252
4. Orava J, Nuutila P, Lidell Martin E et al (2011) Different metabolic responses of human brown adipose tissue to activation by cold and insulin. Cell Metab 14:272–279
5. Xu L, Kanasaki K, Kitada M, Koya D (2012) Diabetic angiopathy and angiogenic defects. Fibrogen Tissue Rep 5: https://doi.org/10.1186/1755-1536-5-13
6. Cinti S (2012) The adipose organ at a glance. Dise Model Mech 5:588–594
7. Lenzen S (2008) The mechanisms of alloxan- and streptozotocin-induced diabetes. Diabetologia 51:216–226
8. Tekabe Y, Johnson LL, Rodriquez K, Li Q, Backer M, Backer JM (2018) Selective imaging of vascular endothelial growth factor receptor-1 and receptor-2 in atherosclerotic lesions in diabetic and non-diabetic apoe−/− mice. Mol Imaging Biol 20:85–93
9. Mirbolooki MR, Constantinescu CC, Pan M-L, Mukherjee J (2011) Quantitative assessment of brown adipose tissue metabolic activity and volume using ^{18}F-FDG PET/CT and β3-adrenergic receptor activation. EJNMMI Res 1:30. https://doi.org/10.1186/2191-219X-1-30
10. Lindholm H, Brolin F, Jonsson C, Jacobsson H (2014) Effects on the FDG distribution by a high uptake of brown adipose tissue at PET examination. EJNMMI Res 4:72. https://doi.org/10.1186/s13550-014-0072-0
11. de Boer SA, Spoor DS, Slart RHJA, et al. (2018) Performance evaluation of a semi-automated method for [^{18}F]FDG uptake in abdominal visceral adipose tissue. Mol Imaging Biol https://doi.org/10.1007/s11307-018-1211-1
12. Ran C, Albrecht DS, Bredella MA, et al. (2017) PET imaging of human brown adipose tissue with the TSPO tracer [^{11}C]PBR28. Mol Imaging Biol https://doi.org/10.1007/s11307-017-1129-z
13. Eriksson O, Mikkola K, Espes D, Tuominen L, Virtanen K, Forsback S, Haaparanta-Solin M, Hietala J, Solin O, Nuutila P (2015) The cannabinoid receptor-1 is an imaging biomarker of brown adipose tissue. J Nucl Med 56:1937–1941
14. Clerte M, Baron DM, Brouckaert P et al (2013) Brown adipose tissue blood flow and mass in obesity: a contrast ultrasound study in mice. J Am Soc Echocardiog 26:1465–1473
15. Nakayama A, Bianco AC, Zhang C-Y, et al. (2003) Quantitation of brown adipose tissue perfusion in transgenic mice using near-infrared fluorescence imaging. Mol imaging. 2: https://doi.org/10.1162/15353500200303103
16. Crane JD, Mottillo EP, Farncombe TH, Morrison KM, Steinberg GR (2014) A standardized infrared imaging technique that specifically detects ucp1-mediated thermogenesis in vivo. Mol Metab 3:490–494
17. Reber J, Willershäuser M, Karlas A, Paul-Yuan K, Diot G, Franz D, Fromme T, Ovsepian SV, Bézière N, Dubikovskaya E, Karampinos DC, Holzapfel C, Hauner H, Klingenspor M, Ntziachristos V (2018) Non-invasive measurement of brown fat metabolism based on optoacoustic imaging of hemoglobin gradients. Cell Metab 27:689–701
18. Chan XHD, Balasundaram G, Attia ABE, Goggi JL, Ramasamy B, Han W, Olivo M, Sugii S (2018) Multimodal imaging approach to monitor browning of adipose tissue in vivo. J Lipid Res 59:1071–1078
19. Deán-Ben XL, Fehm TF, Ford SJ, Gottschalk S, Razansky D (2017) Spiral volumetric optoacoustic tomography visualizes multi-scale dynamics in mice. Light: Sci App 6:e16247
20. Fehm TF, Deán-Ben XL, Ford SJ, Razansky D (2016) In vivo whole-body optoacoustic scanner with real-time volumetric imaging capacity. Optica 3:1153–1159
21. Xu M, Wang LV (2005) Universal back-projection algorithm for photoacoustic computed tomography. Phys Rev E 71:016706
22. Dean-Ben XL, Ozbek A, Razansky D (2013) Volumetric real-time tracking of peripheral human vasculature with GPU-accelerated three-dimensional optoacoustic tomography. IEEE Trans Med Imaging 32:2050–2055
23. Jacques SL (2013) Optical properties of biological tissues: a review. Phys Med Biol 58:R37–R61
24. Razansky D (2012) Multispectral optoacoustic tomography—volumetric color hearing in real time. IEEE J Sel Topics Quant 18:1234–1243
25. Nnodim JO, Lever JD (1988) Neural and vascular provisions of rat interscapular brown adipose tissue. Am J Anat 182:283–293

26. Otsu N (1979) A threshold selection method from gray-level histograms. IEEE Trans Syst Man Cyb 9:62–66
27. Deán-Ben XL, Razansky D (2013) Portable spherical array probe for volumetric real-time optoacoustic imaging at centimeter-scale depths. Opt Express 21:28062–28071
28. Deán-Ben XL, Razansky D (2014) Adding fifth dimension to optoacoustic imaging: volumetric time-resolved spectrally enriched tomography. Light Sci Appl 3:e137
29. Deán-Ben XL, Razansky D (2016) On the link between the speckle free nature of optoacoustics and visibility of structures in limited-view tomography. Photo-Dermatology 4:133–140
30. Deán-Ben XL, López-Schier H, Razansky D (2017) Optoacoustic micro-tomography at 100 volumes per second. Sci Rep 7:6850
31. Deán-Ben X, Fehm TF, Razansky D (2014) Universal hand-held three-dimensional optoacoustic imaging probe for deep tissue human angiography and functional preclinical studies in real time. J Vis Exper: JoVE 93:51864